

# Mantle plume: the dynamic setting of the origin of Early Paleozoic mafic dykes in Ziyang, Shaanxi Province, Southern Qinling Block, China

Xiaoqing Chen<sup>1</sup> · Shen Liu<sup>2</sup> · Caixia Feng<sup>2</sup> · Ian M. Coulson<sup>3</sup> · Yan Fan<sup>2</sup> · Kairui Tai<sup>2</sup> · Tianjing Gao<sup>2</sup> · Siyuan Zhang<sup>2</sup>

Received: 26 March 2020 / Revised: 27 March 2020 / Accepted: 1 April 2020 / Published online: 20 April 2020  
© Science Press and Institute of Geochemistry, CAS and Springer-Verlag GmbH Germany, part of Springer Nature 2020

**Abstract** The mafic dykes (dolerites) during the Early Paleozoic are widely spread in Langao-Ziyang, southern Qiling Block, and the investigation on these dykes are very important. Previous studies have mainly focused on the Silurian mafic dykes; however, research on the Earlier Paleozoic mafic dykes is relatively weak at present. Therefore, the overall understanding of the mantle source and genetic dynamic setting during the Early Paleozoic in this area is lacking. To study the accurate age and origin of the Early Paleozoic mafic dykes in Ziyang, southern Shaanxi Province, the mafic dykes from dabacunand Qinmingzhai were selected and the petrology, zircon U–Pb chronology, geochemistry, and Sr–Nd–Hf isotopes were studied. Analysis indicates that the mafic dykes studied are mainly composed of dolerite, and they are the products of the Early Ordovician (475.8–480.7 Ma). Furthermore, the dolerites belong to alkaline rock series, and they are characterized by enrichment in LREE, Rb, Ba, Sr, Nb, ( $^{87}\text{Sr}/^{86}\text{Sr}$ )<sub>i</sub> = 0.7020–0.7050,  $\epsilon_{\text{Nd}}(t)$  = 3.0–4.0,  $\epsilon_{\text{Hf}}(t)$  = 4.5–12.1,  $^{176}\text{Hf}/^{177}\text{Hf}$  = 0.282681–0.282844. This suggests that the mafic dyke were derived from the partial melting of a depleted lithospheric mantle, and the genetic

process is mainly controlled by the mantle plume based on the discussion of the genetic model. Furthermore, the genetic process experienced the separation and crystallization of olivine and clinopyroxene at the same time, with little crustal contamination.

**Keywords** Early Paleozoic · Dolerites · Geochemistry · Origin · Mantle plume

## 1 Introduction

As a result of the collision between the North China Craton (NCC) and Yangtze Block during Late Triassic, for a long time, the Qinling Orogenic Belt has become one of the hot spots of widespread concern and research. Currently, previous studies have shown that the Earlier Paleozoic mafic dyke and alkaline dyke swarms (Zhang et al. 2002, 2007, 433 Ma; Deng et al. 2003; Yan 2005, 413–471 Ma; Chen et al. 2006, 440 Ma; Wang 2007, 2009, 431 Ma; Li 2009; Zhang 2010, 438 Ma; Zou et al. 2011, 440 Ma; Xie et al. 2014, 410 Ma; Chen et al. 2014, 422 Ma; Long 2016, 415–433 Ma; Zhang et al. 2017, 425 Ma), bimodal volcanic rocks (Yan 2005), large-scale mineralization (Chen et al. 1994; Qi et al. 1999; Deng et al. 2003; Tu 2006; Zeng et al. 2007; Tang et al. 2007; Wu et al. 2010; Wei et al. 2016; Zhu 2017), rift valley and fault basin (Yang 1985; Kuang et al. 1995; Zhang et al. 2001, 2012; Zeng et al. 2007; Tang et al. 2007), thrust nappe structure (Zhang et al. 2001; Liu 2008), and metamorphic core complex (Zhang and Zheng 1999) are widely spread in the Southern Qinling Region. The above typical geological features indicate that the South Qinling Block was in a strong lithospheric extension stage during the Early Paleozoic. At the present, though some studies have been made on the Eearly

✉ Xiaoqing Chen  
chenxq08@163.com

Shen Liu  
liushen@nwu.edu.cn

<sup>1</sup> College of Earth Science, Jilin University, Changchun 130061, China

<sup>2</sup> State Key Laboratory of Continental Dynamics and Department of Geology, Northwest University, Xi'an 710069, China

<sup>3</sup> Solid Earth Studies Laboratory, Department of Geology, University of Regina, Regina, SK S4S 0A2, Canada

Paleozoic lithospheric extensional characteristics in Southern Qinling Block, there is still a lack of systematic studies on the lithospheric extension period, mantle source, and genetic dynamic setting in the extensional setting. Further relevant research thus is necessary. As a representative product of lithospheric extension and fragmentation, mafic dyke swarms are mafic rock assemblages with the same/similar occurrence in the same magmatic event under the background of crustal extension, and the rock composition mainly includes lamprophyre, dolerite, and diabase porphyry (Shao and Zhang 2002; Liu et al. 2010a, b, c). Furthermore, the investigation on these rocks has special research significance (Hall 1982; Li 1990; Li et al. 1997; Shao and Zhang 2002; Xie 2003; Zhao 2004; Zhao et al. 2004; Peng et al. 2004; Yan 2005; Liu et al. 2004, 2006, 2008a, b, 2009, 2010a, b, c, 2012a, b, 2013a, b, c, d, e, f, 2015, 2016, 2017a, b, 2018; Wang et al. 2008; Feng 2012; Yang 2012, 2013; Tang 2013). At present, the research period of the Early Paleozoic mafic rocks in the South Qinling Block is mainly concentrated in the Silurian (410–440 Ma); by contrast, the understanding of the mafic dykes in the extensional setting during the Ordovician and Cambrian is still weak. In this paper, mineralogy, LA-ICP-MS zircon U-Pb dating, rock and isotope (Sr-Nd-Hf) geochemistry are used. The origin and geodynamic setting of the mafic dykes during Ordovician (476–481 Ma) from Ziyang area were discussed.

## 2 Regional geological backgrounds and petrological characteristics

As a very important intercontinental orogenic belt across the east and west of China, Qinling Orogenic Belt is generally divided into three parts: the southern margin of the North China Block, the northern margin of the Yangtze Block and the southern Qinling Block by Shangdan and Mianlue suture zones (Yan 2005). Meanwhile, Qinling Orogenic Belt can be further divided into the southern margin of the North China massif, the thick-skinned imbricate thrust belt of the North Qinling Block, the foreland thrust fold belt of the Qinling Orogenic Belt, the giant nappe front thrust belt of the southern margin of the Bashan-Dabie Mountains, the northern thrust nappe belt of the South Qinling Block, the arc thrust nappe system of the Bashan Mountains in the South Qinling Orogenic Belt, the Nandan fault system and the Mianlue fault (Zhang et al. 2001).

The South Qinling Block is mainly located between the Shangdan Fault zone and the Mianlue-Bashan Arc Fault zone. The West of this block corresponds to the West Qinling and Qaidam massif, and the East includes Wudang, Suizhou, and Tongbai-Dabie block. The south Qinling Block belongs to the northern margin of the Yangtze Plate Pre-Late

Paleozoic. Subsequently, with the opening of the Mianlue oceanic basin in the Late Paleozoic, it gradually separated and formed a relatively independent micro-plate. But until the Early Mesozoic, with the collision and amalgamation with the North China and Yangtze Plates, it eventually became an important part of the Qinling Orogenic Belt (Zhang et al. 2001; Yan 2005). Paleozoic magmatic rocks mainly occur in Langao-Ziyang area south of Ankang, South Qinling Block. The area studied in this study is located in Ziyang Daba village and Qingmingzhai area (southern Ankang), South Qinling Block. The outcropped strata mainly include the Cambrian, Early-Middle Ordovician and Early Silurian (Fig. 1). The main exposed rocks in South Qinling Block include mafic dyke, gabbro, alkaline complex and granitic rocks (Wang 2007). The mafic dykes occur as dykes with NW-SE orientations, and the dykes studied were mainly composed of dolerites, which intrude the Cambrian and Early Ordovician sedimentary basement rocks. Single dykes can range between 4.0 and 110 km in length and 0.6–8.0 km in width (Figs. 2, 3). All of the dolerites are characterized by black-gray and grey-green, massive (with a small number of bubbles), medium-fine texture, the dolerites studied diabasic with secondary-authentic 30 %–36 % clinopyroxene, (3.0–5.0 mm), 65 %–70 % plagioclase (2.0–4.0 mm), olivine, biotite, quartz, apatite, magnetite, and ilmenite (Fig. 3). Moreover, the clinopyroxene is usually altered into a mixture of chlorite, amphibole, and carbonate, and plagioclase is partly replaced by albite, epidote, and kaolinite. Surrounding rocks in the study area mainly includes thick striped silty limestone with silty limestone and lens of bioclastic limestone of the Cambrian Maobaguan Formation, thin-layer fine-grained limestone and bioclastic limestone intercalated with grey medium-thick silty limestone of Baguamiao Formation, thick to super-thick gravel limestone, beaded limestone with muddy streaked siltstone, grey calcareous slate with siltstone, muddy limestone and sandy clastic limestone of Heishuihe Formation. The Ordovician Gaoqiao Formation lime-green viscous slate with silt marl, beaded micrite and banded calc-viscous slate interblended, gray viscous slate, calc-viscous slate with limestone thin beds, black-gray striped viscous slate of Quanhukou Formation with carbonaceous siliceous viscous slate, feldspar quartz sandstone and siltstone. The Silurian porphyry viscous slate, carbonaceous viscous slate, silty slate, silty slate with feldspar quartz siltstone also was found (Fig. 1).

## 3 Analytical methods

### 3.1 U-Pb dating by LA-ICP-MS

Zircon grains from three of the investigated dolerite samples studied (DBC-1, DBC-2, and DBC-3) in Shaanxi

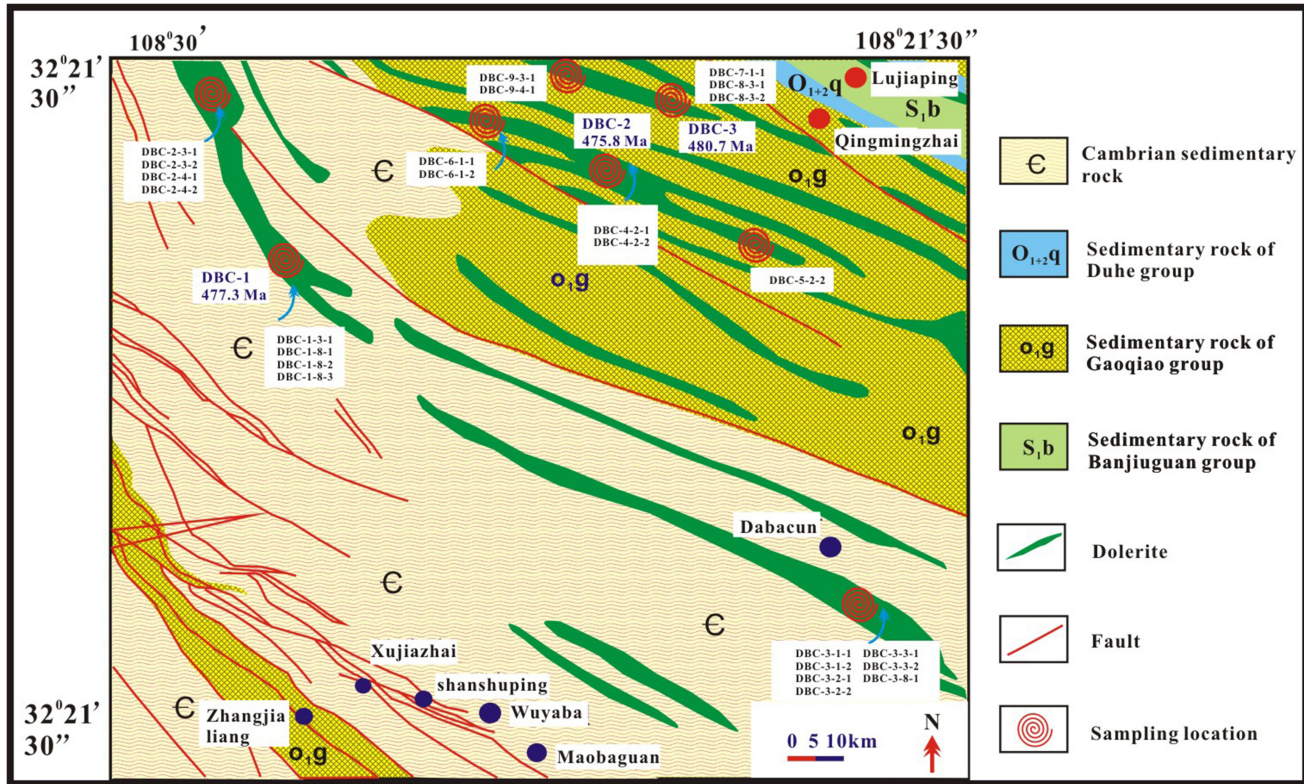


**Fig. 1** The regional geological map and the distribution of the dolerites studied

**Fig. 2** The field Profile of dolerites studied



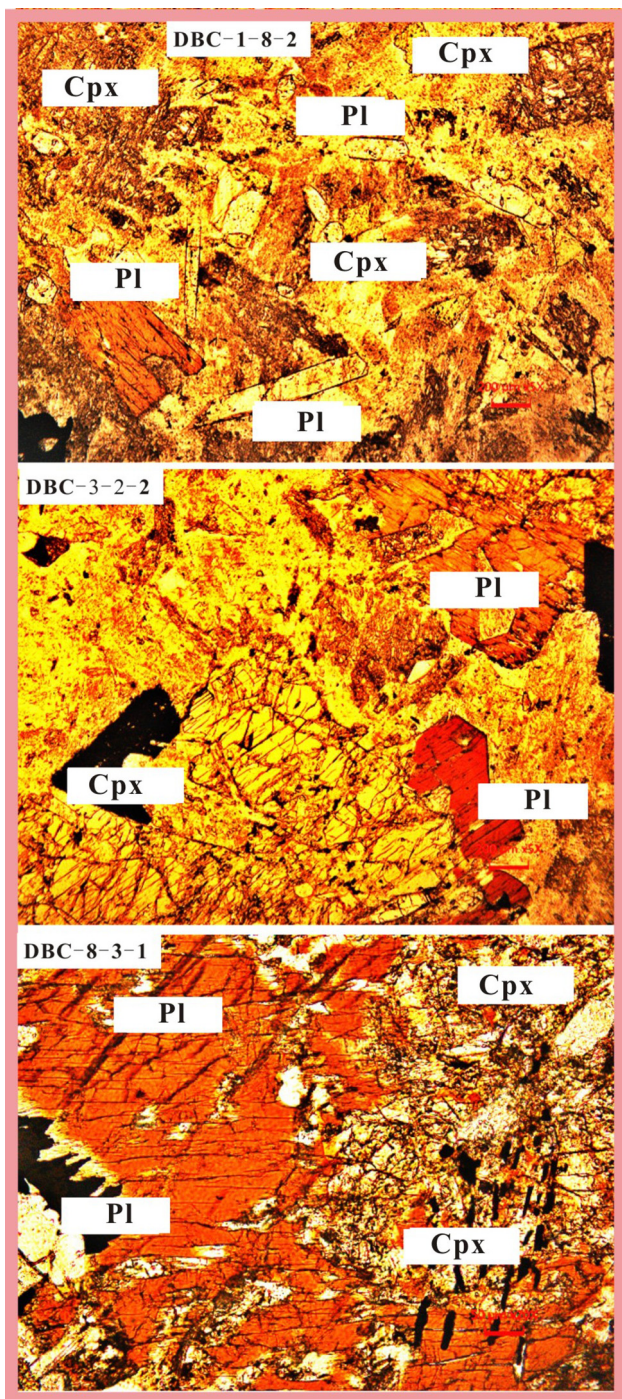


**Fig. 3** The microscopic photos of the dolerite thin sections in the study area. Cpx: clinopyroxene; Pl: plagioclase

Province were separated using conventional heavy liquid and magnetic techniques. Representative zircon was then hand-picked under a binocular microscope before being mounted in an epoxy resin disc, polished, and then coated

with gold prior to analysis. Zircons were documented with transmitted and reflected light as well as cathodoluminescence images to reveal their external and internal structures at the State Key Laboratory of Continental Dynamics, Northwest University. Laser ablation techniques were used for zircon age determinations (Table 1). The analyses were conducted with an Agilent 7500a ICPMS equipped with 193 nm excimer lasers, which is housed at the State Key Laboratory of Geological Processes and Mineral Resources, China University of Geoscience in Wuhan. Zircon 91500 was used as a standard and NIST 610 was used to optimize the results. The spot diameter was 24  $\mu\text{m}$ . The analytical methodology is described in detail in Liu et al. (2007) and Yuan et al. (2004). Common-Pb corrections were made using the method of Andersen (2002). Data were processed using the GLITTER and ISOPLOT (Ludwig, 2003) programs. Errors on individual analyses by LA-ICP-MS are quoted at the 95 % ( $1\sigma$ ) confidence level (Fig. 4).

### 3.2 Major elemental and trace elemental analyses

Major element compositions were determined using analytical Axioms-advanced X-ray fluorescence (XRF) spectrometer at the State Key Laboratory of Ore Deposit Geochemistry (LODG), with an analytical precision of better than 5 %. Trace element compositions were determined by Inductively-coupled plasma mass-spectrometry (ICP-MS) utilizing a Perkin-Elmer ELAN DRC- instrument at the LODG. Prior to analysis, powdered samples (50 mg) were dissolved in high-pressure Teflon bombs, using an HF+HNO<sub>3</sub> attack for 48 h at about 190 °C (Qi et al. 2000). Moreover, signal drift during the analysis was monitored using Rh as an internal standard. GBPG-1, OU-6, GSR-1, and GSR-3 standards were used for analytical quality control with a determined analytical precision of better than 5 %.

### 3.3 Sr–Nd–Hf isotopic analyses

For the analysis of Rb–Sr and Sm–Nd isotopes, sample powders were spiked with mixed isotope tracers, dissolved in Teflon capsules with HF+HNO<sub>3</sub> acids, and separated by conventional cation-exchange techniques. Isotopic measurements were performed using a Finnigan Triton Ti thermal ionization mass spectrometer (TIMS) at the LODG. Procedural blanks were < 200 pg for Sm and Nd, as well as < 500 pg for Rb and Sr. Mass fractionation corrections for Sr and Nd isotopic ratios were based on <sup>86</sup>Sr/<sup>88</sup>Sr = 0.1194 and <sup>146</sup>Nd/<sup>144</sup>Nd = 0.7219, respectively. Analyses of standards yielded the following results:

**Table 1** The composition of the zircon U–Pb dating by LA-ICP-MS for the dolerites studied

DBC-1	Isotopic						Ratios						Age (Ma)				
	Spot	Th	U	Pb	Th/U	$^{238}\text{U}/^{232}\text{Th}$	$^{207}\text{Pb}/^{206}\text{Pb}$	$^{207}\text{Pb}/^{235}\text{U}$	$^{206}\text{Pb}/^{238}\text{U}$	$\delta$	$^{207}\text{Pb}/^{235}\text{U}$	$\delta$	$^{207}\text{Pb}/^{206}\text{Pb}$	$\delta$	$^{206}\text{Pb}/^{238}\text{U}$	$\delta$	
1	1447	660	660	2.16	0.39	0.0593	0.0013	0.6288	0.0212	0.0764	0.0015	589	48.1	495	13.2	474	9
2	2233	954	1046	2.34	0.38	0.0616	0.0018	0.6620	0.0262	0.0773	0.0014	661	61.1	516	16	480	8
3	4469	1415	1845	3.16	0.32	0.0586	0.0014	0.6178	0.0190	0.0762	0.0014	554	54.6	488	11.9	473	8
4	6655	2440	2723	2.73	0.30	0.0579	0.0010	0.6086	0.0178	0.0761	0.0018	524	37	483	11.3	473	11
5	4013	1998	1963	2.01	0.20	0.0573	0.0010	0.6062	0.0160	0.0765	0.0015	506	38.9	481	10.1	475	9
6	8590	3921	3899	2.19	0.17	0.0564	0.0008	0.6025	0.0142	0.0774	0.0015	465	31.5	479	8.97	481	9
7	1277	608	590	2.10	0.38	0.0574	0.0016	0.6045	0.0204	0.0760	0.0011	509	63	480	12.9	472	7
8	1990	838	929	2.37	0.34	0.0584	0.0012	0.6045	0.0151	0.0750	0.0013	546	46.3	480	9.54	466	8
9	2097	726	947	2.89	0.27	0.0567	0.0013	0.5931	0.0170	0.0757	0.0012	480	51.8	473	10.8	470	7
10	1882	878	874	2.14	0.38	0.0569	0.0012	0.6268	0.0185	0.0796	0.0015	500	78.7	494	11.6	494	9
11	1949	725	889	2.69	0.29	0.0571	0.0012	0.6060	0.0154	0.07769	0.0015	498	44.4	481	9.73	478	9
12	991	456	456	1.75	0.44	0.0553	0.0014	0.5896	0.0164	0.0773	0.0013	433	55.6	471	10.5	480	8
13	1491	766	856	1.95	0.36	0.0553	0.0010	0.5931	0.0131	0.0777	0.0013	433	40.7	473	8.37	483	8
14	6271	2847	3184	2.20	0.35	0.0556	0.0010	0.5897	0.0121	0.0768	0.0012	439	38.9	471	7.72	477	7
15	1491	766	735	1.95	0.40	0.0556	0.0014	0.6102	0.0169	0.0795	0.0013	439	55.6	484	10.7	493	8
DBC-2																	
1	1995	748	867	2.67	0.29	0.0555	0.0012	0.6003	0.0138	0.0784	0.0011	432	48	477	9	487	7
2	1308	631	605	2.07	0.37	0.0571	0.0015	0.6200	0.0179	0.0786	0.0011	494	56	490	11	488	6
3	1703	624	751	2.73	0.29	0.0570	0.0013	0.6258	0.017	0.0795	0.0012	500	52	493	11	493	7
4	2072	1014	959	2.04	0.38	0.0598	0.0017	0.6269	0.0207	0.0759	0.0012	594	61	494	13	471	7
5	5031	2229	2235	2.26	0.35	0.0553	0.0010	0.5775	0.0128	0.0757	0.0013	433	39	463	8	471	8
6	1354	728	649	1.86	0.42	0.0543	0.0013	0.5064	0.0167	0.0795	0.0013	383	52	475	11	493	8
7	1080	541	476	2.00	0.40	0.0560	0.0014	0.5825	0.0185	0.0753	0.0013	454	57	466	12	468	8
8	1076	571	499	1.89	0.43	0.0563	0.0014	0.6017	0.0219	0.0771	0.0015	461	56	478	14	479	9
9	2859	1174	1310	2.43	0.32	0.0558	0.0010	0.5972	0.0158	0.0775	0.0015	443	8	475	10	481	9
10	1328	609	601	2.18	0.43	0.0552	0.0014	0.5849	0.0182	0.0768	0.0011	420	55	468	12	477	7
11	2254	889	996	2.54	0.31	0.0532	0.0012	0.5585	0.0143	0.0761	0.0011	339	50	451	9	473	7
12	3776	1233	1600	3.06	0.34	0.0539	0.0012	0.5860	0.0167	0.0788	0.0011	365	47	468	11	489	7
13	2792	1037	1298	2.69	0.30	0.0541	0.0010	0.5756	0.0136	0.0770	0.0011	376	44	462	9	478	6
14	821	461	391	1.78	0.44	0.0522	0.0013	0.5671	0.0167	0.0787	0.0012	295	57	456	11	488	7
15	1574	708	695	2.22	0.36	0.0545	0.0016	0.5717	0.0176	0.0761	0.0012	391	63	459	11	473	7
16	1520	781	682	1.95	0.41	0.0558	0.0013	0.5871	0.0168	0.0762	0.0012	456	54	469	11	474	7
17	569	362	258	1.57	0.51	0.0519	0.0016	0.5432	0.0197	0.0758	0.0012	280	70	441	13	471	7
18	4823	1815	2234	2.66	0.30	0.0540	0.0012	0.5843	0.0172	0.0783	0.0013	372	48	467	11	486	8

Table 1 continued

DBC-1	Isotopic			Ratios			Age (Ma)					
	Spot	Th	U	Pb	Th/U	$^{238}\text{U}/^{232}\text{Th}$	$^{207}\text{Pb}/^{206}\text{Pb}$	$^{207}\text{Pb}/^{235}\text{U}$	$^{206}\text{Pb}/^{238}\text{U}$	$^{207}\text{Pb}/^{206}\text{Pb}$	$^{207}\text{Pb}/^{235}\text{U}$	$^{206}\text{Pb}/^{238}\text{U}$
<b>DBC-3</b>												
1	1995	748	867	2.67	0.29	0.0555	0.0012	0.6003	0.0138	0.0784	0.0012	432
2	1308	631	605	2.07	0.37	0.0571	0.0015	0.6200	0.0179	0.0786	0.0011	494
3	1703	624	751	2.73	0.54	0.0570	0.0013	0.6258	0.0170	0.0795	0.0012	500
4	3397	1359	1623	2.5	0.62	0.0575	0.0014	0.6226	0.0180	0.0782	0.0011	522
5	2072	1014	959	2.04	0.71	0.0598	0.0017	0.6269	0.0207	0.0759	0.0012	594
6	3145	1279	1462	2.46	0.79	0.0556	0.0011	0.6108	0.0162	0.0795	0.0014	435
7	5031	2229	2235	2.26	0.87	0.0553	0.0010	0.5775	0.0128	0.0757	0.0013	433
8	1354	728	649	1.86	0.42	0.0543	0.0013	0.5964	0.0167	0.0795	0.0013	383
9	1080	541	476	2.00	0.40	0.0560	0.0014	0.5825	0.0185	0.0753	0.0013	454
10	1076	571	499	1.89	0.43	0.0563	0.0014	0.6017	0.0219	0.0771	0.0015	461
11	2859	1174	1310	2.43	0.32	0.0558	0.0010	0.5972	0.0158	0.0775	0.0015	443
12	1328	609	601	2.18	0.43	0.0552	0.0014	0.5849	0.0182	0.0768	0.0011	420
13	2254	889	996	2.54	0.31	0.0532	0.0012	0.5585	0.0143	0.0761	0.0011	339
14	3776	1233	1600	3.06	0.34	0.0539	0.0012	0.5860	0.0167	0.0788	0.0011	365
15	2792	1037	1298	2.69	0.30	0.0541	0.0010	0.5756	0.0136	0.0770	0.0011	376
16	821	461	391	1.78	0.44	0.0522	0.0013	0.5671	0.0170	0.0787	0.0010	295
17	1574	708	695	2.22	0.36	0.0545	0.0016	0.5717	0.0180	0.0761	0.0010	391
18	1520	781	682	1.95	0.41	0.0558	0.0013	0.5871	0.0170	0.0762	0.0010	456
19	569	362	258	1.57	0.51	0.0519	0.0016	0.5432	0.0200	0.0758	0.0010	280
20	4823	1815	2234	2.66	0.30	0.0540	0.0012	0.5843	0.0172	0.0783	0.0013	372

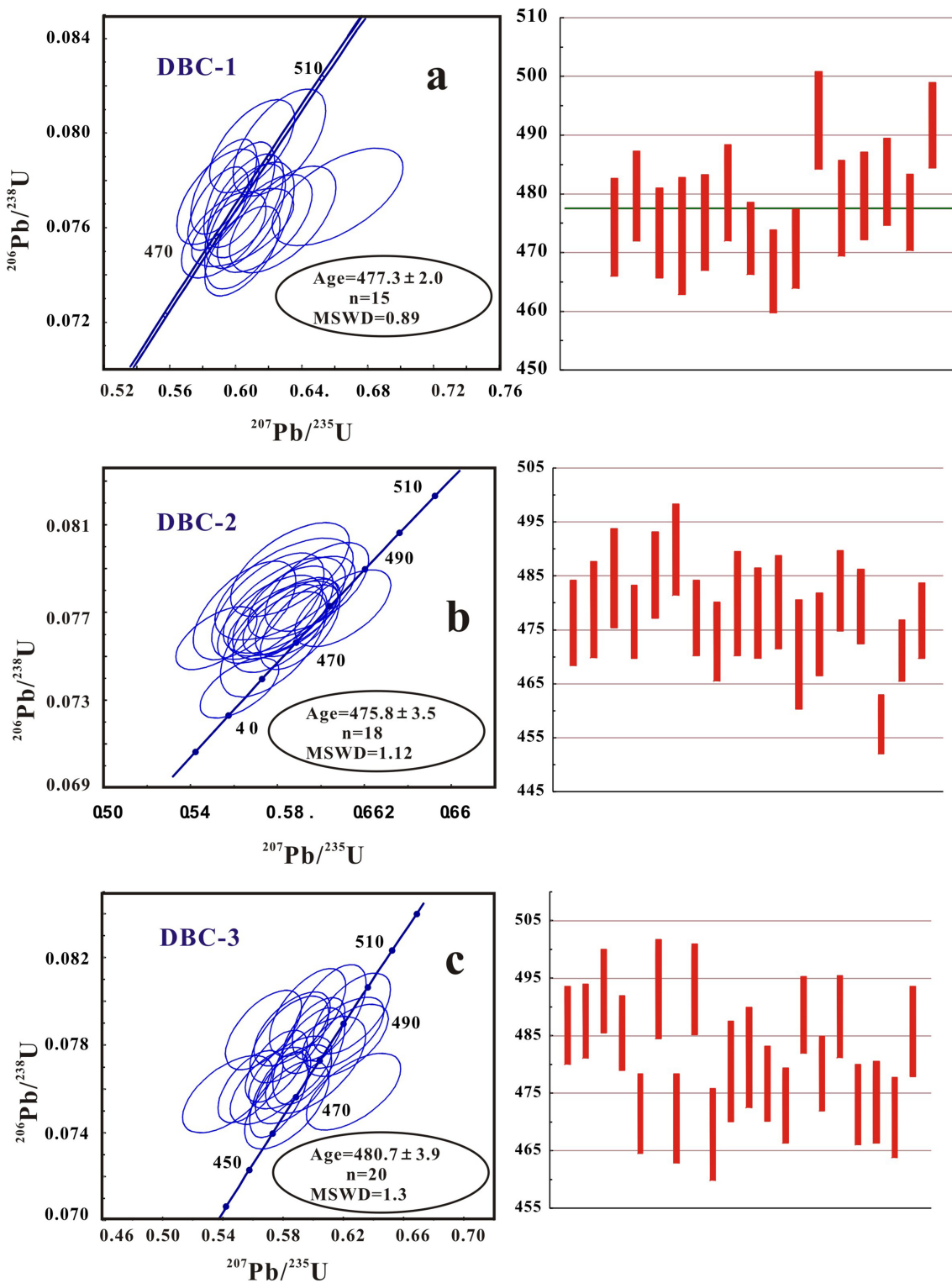


**Fig. 4** The LA-ICP-MS zircon U–Pb dating of the dolerites studied

NBS987 gave  $^{87}\text{Sr}/^{86}\text{Sr} = 0.710246 \pm 16$  ( $2\sigma$ ) and La Jolla gave  $^{143}\text{Nd}/^{144}\text{Nd} = 0.511863 \pm 8$  ( $2\sigma$ ). The analytical results for Sr–Nd isotopes are presented in Table 4.

*In-situ* zircon Hf isotopic analyses were undertaken using a multi-collector-inductively coupled plasma-mass spectrometer equipped with a Geolas-193 laser at the Key

Laboratory of Continental Dynamics, Northwest University. These analyses used a laser repetition rate of 10 Hz at 100 mJ and a beam diameter of either 32 or 63  $\mu\text{m}$ . The isobaric interference of  $^{176}\text{Lu}$  on  $^{176}\text{Hf}$  was corrected by measuring the intensity of the interference-free  $^{175}\text{Lu}$  isotope and using a recommended  $^{176}\text{Lu}/^{175}\text{Lu}$  ratio of 0.02655 (Machado and Simonetti 2001). A  $^{176}\text{Yb}/^{172}\text{Yb}$  value of 0.5887 (Chu et al. 2002) and mean  $\beta_{\text{Yb}}$  values obtained during Hf analysis were used to correct for the interference of  $^{176}\text{Yb}$  on  $^{176}\text{Hf}$  (Iizuka and Hirata 2005). Details of the analytical and data correction procedures are given in Wu et al. (2006). Our analyses included measurements of standard 91,500 and FM0411 zircons, yielding mean  $^{176}\text{Hf}/^{177}\text{Hf}$  ratios of  $0.282313 \pm 36$  [2 standard deviations (SD),  $n = 35$ ] and  $0.282996 \pm 31$  (2SD,  $n = 9$ ), respectively, which agree with the reported  $^{176}\text{Hf}/^{177}\text{Hf}$  composition of the 91500 zircon ( $0.282306 \pm 8$ , 2SD,  $n = 30$ ) by solution analysis (Woodhead et al. 2004) and  $0.282983 \pm 17$  (2SD,  $n = 9$ ) for the FM0411 zircon by *in-situ* analysis (Wu et al. 2006).

## 4 Results

### 4.1 Zircon U–Pb geochronology

Characterization of CL images indicates that selected dating zircons have complete automorphism and are generally columnar with obvious magmatic zones. The Th (501–8590 ppm) and U (362–3921 ppm) composition are relatively high; the range of Th/U ratio is between 1.57 and 8.54 (Table 1). As a result, the chronological zircon cathodoluminescence photographs are darker (Ewing 1994). Also, there is no inherited zircon in zircon grains. Euhedral zircon grains in samples DBC-1, DBC-2, and DBC-3 were observed to be clean and prismatic, with evident oscillatory zoning, suggestive that these were the products of magmatic crystallization. A total of 15 zircon grains provided a weighted mean  $^{206}\text{Pb}/^{238}\text{U}$  age of  $477.3 \pm 2.0$  Ma ( $1\sigma$ ) (95 % confidence interval, MSWD = 0.89) for DBC-1; 18 zircon grains gave a weighted mean  $^{206}\text{Pb}/^{238}\text{U}$  age of  $475.8 \pm 3.5$  Ma ( $1\sigma$ ) (95 % confidence interval, MSWD = 1.12) for DBC-2; 20 grains gave a weighted mean  $^{206}\text{Pb}/^{238}\text{U}$  age of  $480.7 \pm 3.9$  Ma ( $1\sigma$ ) (95 % confidence interval, MSWD = 1.3) for DBC-3. These determinations are the best estimates of the crystallization ages of the dolerites investigated.

### 4.2 Major and trace elements

Whole-rock geochemical data for the dolerites studied in Tables 2 and 3. The dolerite samples exhibit a fairly wide range of compositions:  $\text{SiO}_2$  (41.72–45.23 wt%),  $\text{TiO}_2$

(3.02–5.52 wt%),  $\text{Al}_2\text{O}_3$  (12.26–18.52 wt%),  $\text{Fe}_2\text{O}_3$  (12.15–15.69 wt%),  $\text{MnO}$  (0.14–0.24 wt%),  $\text{MgO}$  (3.27–5.98 wt.%),  $\text{CaO}$  (9.05–11.32 wt%),  $\text{Na}_2\text{O}$  (2.90–3.98 wt%),  $\text{K}_2\text{O}$  (0.40–1.55 wt%),  $\text{P}_2\text{O}_5$  (0.42–0.143 wt%), and  $\text{Mg}^{\#}$  (36–48), and a medium ignition (LOI, 2.62–4.18) (Table 2). The dolerite samples studied all fall into the alkaline field in terms of the total alkali-silica (TAS) diagram (Fig. 5). The dolerites studied exhibit negative correlations between  $\text{SiO}_2$  and  $\text{TiO}_2$ ,  $\text{Fe}_2\text{O}_3$ , and  $\text{MgO}$  (not shown). The samples studied are also characterized by LREE enrichment and HREE depletion, with a wide range of  $\text{Eu/Eu}^*$  ratio (7.75–11.9) and  $(\text{La/Yb})_N$  ratio (7.75–11.5) (Table 3 and Fig. 6a, b). On primitive mantle-normalized trace element diagrams, the dolerites studied show enrichment in LILEs (i.e., Rb, Ba, Th, and Sr), Nb, and Ta, and depletion for Pb, Hf, and Ti (Fig. 6b).

### 4.3 Sr–Nd–Hf isotopes

Sr and Nd isotopic data for 12 representative dolerites studied and Hf isotopic composition for 3 zircon samples (DBC-A, DBC-2, DBC-3) are presented in Tables 4, 5 and Figs. 7, 8. The investigated dolerites show a wide range in  $(^{87}\text{Sr}/^{86}\text{Sr})_{\text{i}}$  values of between 0.7020 to 0.7050 and positive composition in  $\varepsilon_{\text{Nd}}(\text{t})$  values, from 3.0 to 4.0, which suggests source areas with slight depletion. A total of 19 spot analyses were undertaken on sample DBC-1, yielding uniform  $\varepsilon_{\text{Hf}}(\text{t})$  values between 6.4 and 10.5 that correspond to  $T_{\text{DM2}}$  model ages of 908–1279 Ma. A further 19 spot analyses on sample DBC-2 yield another narrow range of  $\varepsilon_{\text{Hf}}(\text{t})$  values between 6.4 and 10.7 and  $T_{\text{DM2}}$  model ages of 770–1040 Ma. A total of 20 spot analyses on sample DBC-3 yielded a relatively wide range of  $\varepsilon_{\text{Hf}}(\text{t})$  values (from 4.5 to 12.1) that correspond to  $T_{\text{DM2}}$  model ages of 571–1450 Ma.

## 5 Discussion

### 5.1 Source, crustal contamination, and fractional crystallization

The dolerites studied were provided with relatively low  $(^{87}\text{Sr}/^{86}\text{Sr})_{\text{i}}$  (0.7020–0.7050), positive  $\varepsilon_{\text{Nd}}(\text{t})$  (3.0–4.0) and  $\varepsilon_{\text{Hf}}(\text{t})$  value (4.5–12.1) (Tables 4, 5; Figs. 7, 8, 9), which indicates that the dykes were derived from partial melting of depleted lithospheric mantle or asthenosphere (e.g., mid-ocean ridge basalt; Liu et al 2016, 2017b). Nevertheless, the dolerites studied are characterized by relatively low Nb/Ta ratio (10.4–12.6), the average is 11.4, and these characteristics are clearly different from those of mid-ocean ridge basalts (Nb/Ta = 17.7; Sun and McDonough 1989). Also, it suggests that magmatic origin may be influenced by crustal contamination (Green 1995). In general, crustal

**Table 2** The major elemental composition of the dolerites studied (wt%)

Sample	Rock type	SiO <sub>2</sub>	TiO <sub>2</sub>	Al <sub>2</sub> O <sub>3</sub>	Fe <sub>2</sub> O <sub>3</sub>	MnO	CaO	MgO	K <sub>2</sub> O	Na <sub>2</sub> O	P <sub>2</sub> O <sub>5</sub>	LOI	Total	Mg <sup>#</sup>
DBC-13-1	Dolerite	43.00	5.06	13.16	14.56	0.23	9.69	5.15	1.21	3.42	0.57	3.21	99.26	44
DBC-1-8-1	Dolerite	42.56	4.37	13.14	14.93	0.24	10.19	4.73	0.83	3.29	1.43	3.55	99.26	41
DBC-1-8-2	Dolerite	42.68	4.42	13.14	14.84	0.24	10.08	4.64	0.83	3.32	1.42	3.60	99.21	41
DBC-1-8-3	Dolerite	42.66	4.43	13.09	14.74	0.24	10.29	4.69	0.84	3.32	1.34	3.64	99.28	41
DBC-2-3-1	Dolerite	43.68	4.66	13.50	13.20	0.21	10.54	5.04	0.83	3.35	0.96	3.00	99.30	46
DBC-2-3-2	Dolerite	42.76	4.88	12.59	14.00	0.22	10.91	5.28	0.77	3.28	0.88	3.34	99.12	45
DBC-2-4-1	Dolerite	42.70	5.11	13.75	14.52	0.22	9.50	4.80	0.94	3.45	0.74	3.55	99.25	42
DBC-2-4-2	Dolerite	43.15	5.16	13.97	14.55	0.22	9.30	4.75	0.85	3.55	0.66	3.53	99.30	42
DBC-3-1-1	Dolerite	41.72	4.89	13.60	14.66	0.22	9.20	4.85	1.55	3.47	0.72	3.15	99.27	42
DBC-3-1-2	Dolerite	42.17	4.96	13.70	14.23	0.22	9.05	4.90	1.49	3.15	0.96	3.38	99.14	43
DBC-3-2-1	Dolerite	42.29	5.38	12.29	15.25	0.24	11.15	5.46	0.76	3.51	0.69	4.32	99.26	44
DBC-3-2-2	Dolerite	42.40	5.20	12.69	15.22	0.23	11.09	5.19	0.64	3.31	0.57	3.24	99.24	43
DBC-3-3-1	Dolerite	42.70	5.22	12.96	15.06	0.23	9.71	5.20	0.66	3.55	0.56	3.72	99.47	43
DBC-3-3-2	Dolerite	42.15	5.52	12.26	15.69	0.24	10.00	5.45	0.56	3.63	0.64	3.62	99.26	43
DBC-3-8-1	Dolerite	43.49	3.02	12.29	15.56	0.21	10.15	5.67	0.74	3.74	0.55	3.23	99.24	45
DBC-4-2-1	Dolerite	42.30	5.15	13.32	14.87	0.22	9.67	5.18	0.63	3.54	0.72	3.83	99.33	43
DBC-4-2-2	Dolerite	42.98	4.95	13.61	14.46	0.22	9.61	4.72	0.73	3.56	0.81	3.74	99.27	42
DBC-4-2-3	Dolerite	45.25	4.45	14.21	12.15	0.21	9.68	3.91	1.19	3.98	0.85	3.63	99.39	41
DBC-5-2-2	Dolerite	42.51	4.43	13.17	14.88	0.24	10.06	4.61	1.24	3.83	1.04	3.51	99.34	41
DBC-6-1-1	Dolerite	44.36	4.78	13.18	13.54	0.21	11.32	5.23	0.40	3.22	0.52	3.34	99.37	46
DBC-6-1-2	Dolerite	42.79	5.10	14.22	14.82	0.20	10.20	4.70	0.66	3.33	0.49	2.62	99.19	41
DBC-7-1-1	Dolerite	43.60	4.88	12.92	14.42	0.21	10.11	5.98	0.65	3.33	0.48	2.68	99.34	48
DBC-8-3-1	Dolerite	42.88	3.41	18.30	12.91	0.14	9.86	3.27	0.56	3.36	0.46	2.75	99.33	36
DBC-8-3-2	Dolerite	42.36	3.39	18.52	12.75	0.15	10.55	3.31	0.77	2.90	0.42	4.18	99.30	38
DBC-9-3-1	Dolerite	43.94	4.77	15.40	13.92	0.18	9.05	4.63	0.87	3.34	0.46	4.19	99.26	46
DBC-9-4-1	Dolerite	42.48	5.05	14.60	14.52	0.22	9.70	4.90	0.78	3.32	0.64	2.68	99.37	46

contamination can result in Nb–Ta depletion and relative enrichment of Sr–Nd isotopes in mafic rocks (Guo et al. 2004). However, these geochemical characteristics have not been observed in the mafic dykes studied (Figs. 6b, 7). Moreover, on the plots of Nb/Ta vs. La/Yb, Ce/Nb vs. Th/Nb, Th/Nb vs. Ta/Yb, and La/Nb vs. Ce/Pb (not shown), no significant correlation was found for the dolerites studied. The obvious crustal contamination thus is negated during the diagenetic process. This is further supported by relatively high Ce/Pb ratio (36–55), positive Nb anomaly, negative Pb anomaly, and lack of inherited zircon (Hofmann 1988; Zhang et al. 2002). It is generally accepted that fractional crystallization is the most important mechanism for the differentiation and evolution of mafic magma. Firstly, fractional crystallization was supported by the low Cr (almost all less than 15.0 ppm), Ni composition, and Mg<sup>#</sup> value (36–48) (Liu et al. 2018). Furthermore, the negative between SiO<sub>2</sub> and TiO<sub>2</sub>, Fe<sub>2</sub>O<sub>3</sub>, and MgO provide credible evidence for the separation of olivine and clinopyroxene. However, separation of plagioclase and Ti-

bearing minerals such as rutile and ilmenite are excluded (Liu et al. 2018).

## 5.2 Genetic model

On La vs. La/Sm plot, the projection point of the dolerites show an obvious positive correlation (Fig. 9), indicating that they were derived from partially melting of a depleted lithospheric mantle. Based on the above discussion, the rising melt was also affected by little crustal contamination during the ascent. Nevertheless, a dynamic model is still needed to explain the origin of these dolerites. At present, there are three possible genetic models for the dolerites studied: (1) contribution of Subduction Yangtze Block (Liu et al. 2018); (2) the role of subduction of the Paleo-Pacific Plate (e.g., the Izenaki Plate); and (3) the dolerites studied may be the product of continental rift environment (Wang 2007). However, it is generally accepted that the final collision between the NCC and Yangtze Block occurred in the Late Triassic (Meng and Zhang 1999; Zhang et al.

**Table 3** The trace elemental composition of the Dolerites studied (ppm)

Sample	Sc	V	Cr	Ni	Ga	Rb	Sr	Y	Zr	Nb	Ba	La	Ce	Pr	Nd	Sm	Eu
	Gd	Tb	Dy	Ho	Er	Tm	Yb	Lu	Hf	Ta	W	Pb	Th	U	Eu/Eu*	(La/Yb)	
DBC-1-3-1	23.0	389	7.38	8.11	20.0	20.3	666	21.9	135	34.5	319	21.7	49.4	6.46	29.6	6.70	2.67
DBC-1-8-1	18.5	366	8.80	7.14	22.2	19.1	665	28.9	154	35.5	322	24.2	51.6	9.09	30.4	6.86	2.91
DBC-1-8-2	18.2	355	4.52	4.88	21.4	19.4	637	27.6	147	34.6	331	20.5	51.8	8.93	29.2	6.92	2.85
DBC-1-8-3	19.1	375	11.2	9.49	22.2	18.8	700	28.6	149	35.3	325	23.6	52.2	9.12	30.4	7.03	2.87
DBC-2-3-1	23.2	358	14.2	10.6	20.7	18.2	643	21.6	132	34.3	251	21.7	49.1	6.39	29.3	6.51	2.76
DBC-2-3-2	23.2	368	6.10	5.89	19.6	18.6	635	21.3	130	36.3	328	20.9	47.4	6.26	28.8	6.45	2.69
DBC-2-4-1	20.1	404	3.53	5.97	21.7	17.4	717	21.6	137	35.5	334	22.4	50.6	6.60	30.0	6.75	2.88
DBC-2-4-2	19.7	399	7.95	7.70	21.5	18.4	710	21.0	140	35.6	336	21.7	48.7	6.35	28.6	6.39	2.73
DBC-3-1-1	19.6	397	8.11	6.10	21.4	20.6	683	21.5	138	34.5	328	21.9	50.1	6.54	29.9	6.73	2.87
DBC-3-1-2	20.1	408	11.8	9.17	21.7	21.3	700	22.5	143	34.4	336	23.5	53.2	6.94	31.4	7.06	2.84
DBC-3-2-1	24.7	453	5.76	7.27	21.5	18.5	670	23.8	137	34.8	275	23.8	50.4	7.02	31.9	6.88	2.76
DBC-3-2-2	22.8	423	11.0	6.25	20.6	17.3	666	22.2	136	35.5	335	22.1	50.4	6.57	30.1	6.81	2.76
DBC-3-3-1	21.9	406	5.26	6.09	20.6	17.9	712	21.1	133	35.2	331	22.1	49.3	6.37	28.8	6.40	2.54
DBC-3-3-2	22.7	440	8.93	7.80	20.2	18.5	608	22.1	131	34.7	248	21.4	48.7	6.31	28.8	6.52	2.58
DBC-3-8-1	21.3	300	58.8	167	17.6	19.4	589	20.2	133	35.2	254	21.3	47.4	5.97	26.3	5.74	2.63
DBC-4-2-1	19.4	373	9.27	6.97	19.6	19.3	614	21.4	128	34.4	289	21.3	48.5	6.35	28.8	6.42	2.58
DBC-4-2-2	20.2	391	7.85	6.51	21.0	19.3	724	22.1	133	33.9	326	23.4	52.6	6.78	30.5	6.84	2.70
DBC-4-2-3	17.0	323	8.42	6.86	20.7	19.5	698	19.5	142	34.4	346	23.4	50.5	6.76	28.6	6.15	2.67
DBC-5-2-2	17.8	361	3.05	5.05	21.2	19.8	618	26.2	140	33.8	318	24.2	51.6	8.48	30.4	6.85	2.71
DBC-6-1-1	23.9	350	6.87	9.07	18.7	19.4	651	19.5	117	32.8	358	19.7	45.6	5.87	26.7	6.02	2.48
DBC-6-1-2	21.0	418	10.0	10.0	21.6	17.9	715	19.5	139	34.3	355	22.3	48.6	6.12	27.1	5.98	2.67
JDBC-7-1-1	26.9	359	4.85	6.51	18.2	20.3	635	20.5	122	32.4	325	19.9	46.3	5.94	27.1	6.25	2.41
DBC-8-3-1	12.8	382	10.4	27.1	22.0	17.8	788	17.4	131	33.6	332	21.9	47.7	5.96	25.8	5.48	2.55
DBC-8-3-1	13.1	393	9.43	28.4	22.6	18.7	784	17.6	128	34.2	338	22.3	48.0	6.02	25.9	5.45	2.48
DBC-8-3-2	13.5	395	9.08	24.4	22.4	18.2	792	17.5	125	32.3	335	21.8	47.4	5.93	25.6	5.41	2.62
DBC-9-3-1	19.4	366	6.89	5.86	20.1	18.4	640	17.6	137	33.6	344	22.3	47.0	5.79	24.9	5.43	2.56
DBC-9-4-1	20.5	393	14.3	10.3	20.6	18.3	738	22.2	139	33.8	360	23.6	52.1	6.98	31.1	7.02	2.71
Sample	Gd	Tb	Dy	Ho	Er	Tm	Yb	Lu	Hf	Ta	W	Pb	Th	U	Eu/Eu*	(La/Yb)	
DBC-1-3-1	6.09	0.95	4.72	0.83	2.17	0.26	1.57	0.21	3.73	3.02	31.0	1.31	1.75	0.39	1.25	9.90	
DBC-1-8-1	8.50	1.26	6.23	1.09	2.80	0.33	1.98	0.27	3.85	3.20	14.4	1.05	2.07	0.46	1.16	8.78	
DBC-1-8-2	8.34	1.23	6.06	1.05	2.75	0.32	1.90	0.26	3.94	3.19	24.8	1.10	2.15	0.43	1.15	7.75	
DBC-1-8-3	8.39	1.25	6.20	1.08	2.78	0.32	1.97	0.26	3.98	3.21	18.0	1.06	2.11	0.45	1.14	8.58	
DBC-2-3-1	5.96	0.92	4.63	0.82	2.13	0.25	1.53	0.21	3.62	2.82	28.9	1.29	1.63	0.38	1.33	10.2	
DBC-2-3-2	6.11	0.92	4.66	0.82	2.14	0.25	1.59	0.22	3.72	2.92	15.8	1.25	1.76	0.38	1.29	9.42	
DBC-2-4-1	6.15	0.95	4.70	0.83	2.18	0.26	1.61	0.22	3.83	3.14	12.5	0.97	1.78	0.39	1.34	9.96	

**Table 3** continued

Sample	Gd	Tb	Dy	Ho	Er	Tm	Yb	Lu	Hf	Ta	W	Pb	Th	U	Eu/Eu*	(La/Yb)
DBC-2-4-2	5.90	0.90	4.52	0.80	2.11	0.25	1.56	0.21	3.83	3.12	21.3	1.10	1.84	0.40	1.33	9.97
DBC-3-1-1	6.14	0.92	4.71	0.82	2.18	0.25	1.60	0.21	3.82	3.05	12.8	1.32	1.80	0.39	1.34	9.79
DBC-3-1-2	6.54	0.97	4.93	0.86	2.27	0.27	1.64	0.22	4.01	3.15	10.6	1.25	1.93	0.41	1.26	10.3
DBC-3-2-1	6.63	1.02	5.13	0.90	2.36	0.29	1.74	0.24	3.83	3.36	41.4	1.26	2.18	0.46	1.23	9.77
DBC-3-2-2	6.25	0.95	4.83	0.86	2.20	0.26	1.62	0.22	3.82	3.10	30.7	1.25	1.74	0.41	1.27	9.77
DBC-3-3-1	5.89	0.90	4.62	0.81	2.11	0.25	1.62	0.22	4.04	3.14	13.9	1.17	2.07	0.42	1.24	9.78
DBC-3-3-2	5.89	0.91	4.48	0.80	2.10	0.25	1.51	0.21	3.83	2.94	15.6	0.98	1.59	0.38	1.25	10.2
DBC-3-8-1	5.36	0.81	4.11	0.73	1.96	0.23	1.44	0.20	3.38	2.88	8.85	1.23	1.59	0.36	1.43	10.6
DBC-4-2-1	5.86	0.90	4.47	0.79	2.04	0.24	1.49	0.20	3.46	2.72	21.0	1.13	1.56	0.36	1.26	10.2
DBC-4-2-2	6.25	0.95	4.75	0.85	2.19	0.26	1.59	0.22	3.96	3.07	32.2	1.18	2.10	0.43	1.24	10.6
DBC-4-2-3	5.65	0.84	4.19	0.74	1.99	0.25	1.55	0.21	4.12	2.89	19.7	1.12	3.44	0.43	1.36	10.8
DBC-5-2-2	7.88	1.18	5.82	1.00	2.54	0.29	1.86	0.25	3.87	3.11	12.6	1.17	1.99	0.38	1.12	9.35
DBC-6-1-1	5.53	0.85	4.27	0.74	1.94	0.23	1.43	0.20	3.28	2.98	20.7	1.26	1.50	0.38	1.29	9.92
DBC-6-1-2	5.49	0.83	4.21	0.73	1.93	0.23	1.43	0.20	3.83	2.96	16.1	1.23	2.41	0.45	1.40	11.2
JDBC-7-1-1	5.76	0.88	4.51	0.79	2.04	0.24	1.48	0.20	3.52	2.96	15.3	0.85	1.74	0.39	1.21	9.65
DBC-8-3-1	4.98	0.74	3.78	0.66	1.80	0.21	1.37	0.19	3.48	2.84	10.5	0.97	2.12	0.43	1.47	11.5
DBC-8-3-1	5.03	0.75	3.77	0.67	1.81	0.23	1.36	0.19	3.41	2.98	10.9	1.06	2.16	0.45	1.42	11.7
DBC-8-3-2	4.98	0.75	3.69	0.66	1.74	0.22	1.32	0.18	3.31	2.91	25.0	0.93	2.05	0.42	1.52	11.9
DBC-9-3-1	4.99	0.74	3.76	0.67	1.76	0.21	1.36	0.18	3.68	3.12	17.3	0.88	2.35	0.44	1.47	11.8
DBC-9-4-1	6.35	0.96	4.85	0.85	2.23	0.26	1.63	0.22	3.81	3.04	18.3	1.26	1.94	0.42	1.22	10.4

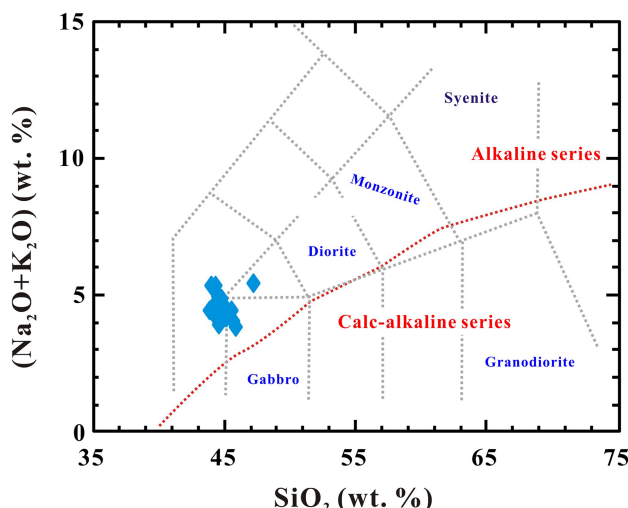


**Fig. 5** The correlation diagram between  $\text{SiO}_2$  vs.  $(\text{Na}_2\text{O}+\text{K}_2\text{O})$  (wt. %) of the dolerites studied

2001; Zhang 2001; Yan 2005). Furthermore, there is no westward subduction of the Paleo-Pacific Plate to the NCC occurred before the Early Cretaceous. Because the mafic dykes did not emplace until the Early Paleozoic, the genesis process thus should not be related to the subduction of the Yangtze lithosphere or the Paleo-Pacific plate. The genetic model of the dolerites studied thus is still pending. At present, although great achievements have been made for Qinling Orogenic Belt, there are still fierce disputes about the Early Paleozoic tectonic evolution of South Qinling Orogenic Belt. Therefore, it is no doubt very important to study the rocks (such as mafic dykes and alkaline complexes) which have obvious indicative effect on structural evolution.

Alkaline complex is widely distributed in South Qinling structural belt, based on petrology, mineralogy and geochemistry investigation, Wang (2007) suggest that these rock belongs to bimodal volcanic rock, and they were formed in a rift tectonic environment, the development of continental rift and associated magmatic activity are related to mantle plume activity, although the deep dynamic characteristics of rift structural exchange need to be further explored. Meanwhile, the continental rift resulted in lithospheric extension. In general, the South Qinling Block is generally in an extensional environment during the Early Paleozoic (700–447 Ma), suggesting that the whole South Qinling has a similar dynamic background at this time (Yan 2005). In general, the extensional tectonic environment is related to the deep slow material movement (or the mantle plume). When the rift extends to a certain extent, the lower slow material will rise to the upper crust or the surface of the crust along the relevant region due to the weakening of the upper crustal stress, and then form large-

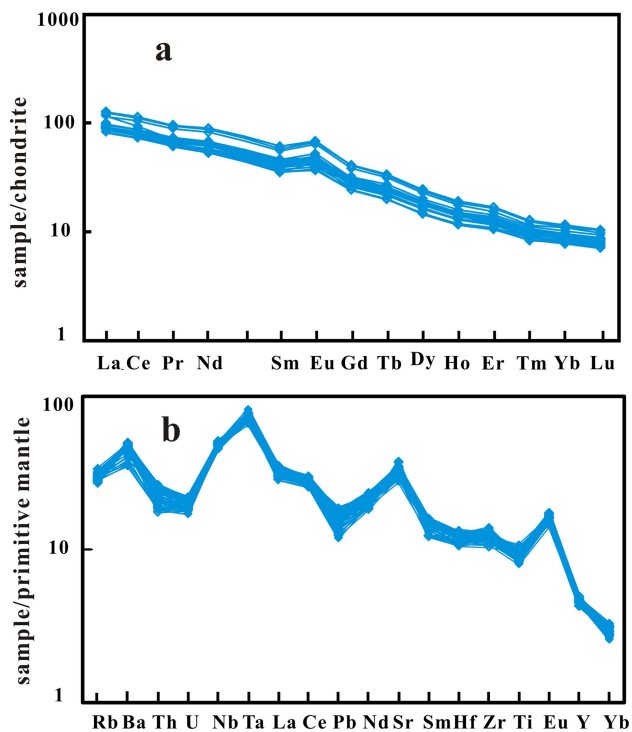


**Fig. 6** The Chondrite normalized REE pattern and Primitive mantle normalized trace element pattern of the dolerites from the study area (Sun and McDonough 1989)

scale mafic dyke swarms, alkaline rock, and bimodal volcanic rock (Yan 2005; Liu et al. 2004, 2006, 2008a, b, 2009, 2010a, b, 2012a, b, 2013a, b, c, f, 2015, 2016, 2017a, b, 2018).

At present, the mantle plume theory has been successfully applied to the continental dynamics (e.g., lithospheric extension, and rift) (Morgan 1971; Condie 1976; Hofmann and White 1982; Breithopf 1989; Griffiths and Campbell 1990; Hill et al. 1992; Davies and Richards 1992; Hull 1993; White and Kenzie 1995; Wang et al. 1997; Wedepohl and Baumann 1999; Li et al. 1999; Wang 1998, 2001; Zhang 2001; Xu et al. 2001; Yan 2005; Li and Yang 2011; Thompson and Gibson 2019), geomagnetic polarity, biological extinction, and climate change. There are at least 45 mantle plumes in the world, including 14 on continents and more than 30 on the ocean (e.g., Hawaii, Yellow stone, Iceland, Afar, Pacific Ocean, Atlantic Ocean, Emei, Wang 1998, 2001). Nowadays, the geochemical identification of the basalts from different ages in the Qinling Orogenic Belt indicates that the mantle plume-derived magmatism in the South Qinling Orogenic Belt began in the Late Mesoproterozoic (Zhang et al. 2001). The formation of the mafic-bimodal volcanic rocks, ophiolite, alkaline, and mafic dykes before the Silurian in South Qinling Orogenic Belt is related to the mantle plume

**Table 4** Sr and Nd isotopic composition of the dolerites studied

Sample	Age (Ma)	Rb (ppm)	Sr (ppm)	$^{87}\text{Rb}/^{86}\text{Sr}$	$^{87}\text{Sr}/^{86}\text{Sr}$	$\pm 2\delta$	Sm (ppm)	Nd (ppm)	$^{147}\text{Sm}/^{144}\text{Nd}$	$^{143}\text{Nd}/^{144}\text{Nd}$	$\pm 2\delta$	$^{87}\text{Sr}/^{86}\text{Sr}$	$(^{143}\text{Nd}/^{144}\text{Nd})$	$^{87}\text{Nd} (\text{t})$
DBC-1-3-1	477.3	23.3	666	0.101	0.705474	7	6.70	29.6	0.136	0.512628	3	0.704787	0.512202	3.5
DBC-1-8-2	477.3	19.4	637	0.088	0.705425	5	8.96	40.9	0.132	0.512610	5	0.704826	0.512197	3.4
DBC-2-3-2	477.3	15.4	500	0.089	0.705394	6	6.45	28.8	0.135	0.512623	4	0.704790	0.512202	3.5
DBC-2-4-2	477.3	18.4	710	0.075	0.705490	5	6.39	28.6	0.135	0.512620	4	0.704982	0.512200	3.5
DBC-3-1-1	477.3	49.6	683	0.210	0.705938	6	6.73	29.9	0.136	0.512608	5	0.704509	0.512184	3.1
DBC-3-1-2	477.3	53.7	700	0.222	0.705940	5	7.06	31.4	0.135	0.512609	3	0.704429	0.512186	3.2
DBC-3-2-2	477.3	17.3	666	0.279	0.705445	6	6.81	30.1	0.132	0.512620	5	0.703549	0.512207	3.6
DBC-3-3-2	477.3	12.8	608	0.247	0.705323	7	6.52	28.8	0.125	0.512617	3	0.703643	0.512228	4.0
DBC-4-2-1	475.8	16.3	614	0.337	0.705375	6	6.42	28.8	0.141	0.512618	4	0.703089	0.512180	3.0
DBC-6-1-1	475.8	9.43	551	0.391	0.705356	7	6.02	26.7	0.138	0.512618	4	0.702707	0.512186	3.2
DBC-8-3-1	480.7	18.7	940	0.337	0.705416	7	5.45	25.9	0.128	0.512588	5	0.703107	0.512185	3.2
DBC-9-3-1	480.7	25.6	640	0.498	0.705402	6	5.43	24.9	0.127	0.512591	5	0.701992	0.512190	3.3

activity rather than the contribution of lithospheric mantle material (Zhang et al. 2002), which is further supported by the deep-water basins of the Ordovician continental margin rift with rich silicon and carbon were developed on the passive continental margin the Early Paleozoic in South Qinling Block (Wang. 2007), magmatic complex intruded into the sedimentary rock series of the rift, enrichment of LREE, Nb, and Ta, Th/Hf (more than 0.3), lower Th/Ta ratio (0.41–2.68) and depletion of Pb composition (Trevon 1995; Zhang 2001; Xu et al. 2001; Zhang et al. 2002, 2007; Yan 2005; Li and Yang 2011). These characteristics have been shown in the dolerites studied (higher Th/Hf = 0.42–0.63, lower Th/Ta = 0.50–1.19; Table 3), and depletion of Pb (Fig. 6b), suggesting that these dolerites should be the product of the typical magmatic activity of the mantle plume (Zhang 2001; Yan 2005). This is further supported by the multi-stage bimodal sedimentary-volcanic formation and structural variation characteristics of the ophiolite and North China-Yangtze Block in the Qinling Orogenic Belt (Yan 2005).

Previous geochemical identification of mantle source types in different periods of QinlingOrogenic Belt indicates that the magmatic activity of mantle plume in North Qinling Block began in the Paleoproterozoic, while that in South Qinling Block began in the late Mesoproterozoic, and that different mantle plume activities migrated from north to southwith time (Zhang 2001). In the Early Paleozoic, mantle plume activity thus mainly occurred in the Mianlue-Ziyang-Langao line. In the Late Paleozoic, the center of mantle plume activity moved further southward, and a large-scale Emeishan overflow basalt was formed in southwestern China. On Ta/Hf vs. Th/Hf and Th/Zr vs. Nb/Zr plots (not shown), all dolerites studied fall in the field of a mantle plume, the dolerites studied also show characteristics similar to OIB-type basalts on the primitive mantle normalized plot (Fig. 6b). Furthermore, the dolerites studied are characterized by enrichment of Rb, Ba, and Sr and light rare earth elements, Ta/Hf = 0.77–0.91 and Th/Ta = 0.54–1.19 (Table 3). Based on the above discussion, the dolerites studied are the typical product of mantle plume magmatism during the Early Paleozoic. The upwelling of deep mantle plume leads to an extensional extension of the overburden crust; it not only intensifies the activity of the original fracture system but also produces a series of radial fracture systems centered on the axis of a mantle plume. The formed radial fissure system thus becomes an advantageous channel for magma ascension. At the end of magmatism, the unexploded magma emplaced and consolidated to form large-scale radial mafic dyke swarms and related igneous rocks (Zhang et al. 2002, 2007, 2017; Wang 2007; Li 2009; Zhang 2010). The thickness of the lithosphere is large more than 150 km, as low degree, partial melting occurs in the mantle source area

**Table 5** The Hf isotopic composition of the dolerites studied

DBC-1	Spot	$^{176}\text{Yb}/^{177}\text{Hf}$	$^{176}\text{Lu}/^{177}\text{Hf}$	$^{176}\text{Hf}/^{177}\text{Hf}$	$\delta\text{Hf}$	$\epsilon_{\text{Hf}}(\text{t})$	$T_{\text{DM1}}(\text{Ma})$	$T_{\text{DM2}}(\text{Ma})$	$f_{\text{Lu/Hf}}$
	1	0.093942	0.002981	0.282626	0.00004	6.5	847	1269	-0.91
	2	0.082209	0.002483	0.282734	0.00002	8.4	764	1100	-0.93
	3	0.079875	0.002483	0.282770	0.00002	9.6	712	987	-0.93
	4	0.084346	0.002658	0.282757	0.00002	9.1	735	1034	-0.92
	5	0.017813	0.000817	0.282681	0.00002	7.00	806	1224	-0.98
	6	0.081153	0.002524	0.282708	0.00002	7.4	804	1185	-0.92
	7	0.084285	0.002604	0.282680	0.00002	6.4	848	1279	-0.92
	8	0.072494	0.002234	0.282768	0.00002	9.7	710	986	-0.93
	9	0.090457	0.002818	0.282734	0.00002	8.3	771	1110	-0.92
	10	0.093164	0.003074	0.282727	0.00002	8.0	788	1140	-0.91
	11	0.096639	0.002995	0.282725	0.00002	7.9	789	1143	-0.91
	12	0.061437	0.001964	0.282712	0.00002	7.7	787	1158	-0.94
	13	0.055460	0.001809	0.282753	0.00003	9.3	724	1022	-0.95
	14	0.083021	0.002382	0.282728	0.00002	8.2	771	1117	-0.93
	15	0.086485	0.002803	0.282699	0.00009	7.0	824	1222	-0.92
	16	0.107062	0.003277	0.282802	0.00003	10.5	680	908	-0.90
	17	0.093000	0.002866	0.282781	0.00002	9.9	703	963	-0.91
	18	0.028290	0.001204	0.282763	0.00001	9.8	698	972	-0.96
	19	0.084172	0.002396	0.282756	0.00002	9.2	731	1030	-0.93
	DBC-2								
	1	0.118522	0.003753	0.282783	0.00003	9.7	719	834	-0.89
	2	0.062562	0.002205	0.282713	0.00002	7.7	786	956	-0.94
	3	0.057512	0.001863	0.282745	0.00002	8.9	736	880	-0.94
	4	0.115396	0.003623	0.282690	0.00002	6.4	857	1040	-0.89
	5	0.090112	0.002807	0.282746	0.00002	8.7	754	897	-0.92
	6	0.065262	0.002115	0.282724	0.00002	8.1	772	934	-0.94
	7	0.102250	0.003181	0.282781	0.00002	9.8	710	826	-0.90
	8	0.054090	0.001755	0.282722	0.00002	8.1	767	930	-0.95
	9	0.087150	0.002718	0.282794	0.00002	10.4	681	788	-0.92
	10	0.079077	0.002554	0.282735	0.00002	8.3	765	918	-0.92
	11	0.082536	0.002715	0.282717	0.00002	7.7	796	962	-0.92
	12	0.073866	0.002422	0.282769	0.00002	9.6	712	838	-0.93
	13	0.073163	0.002310	0.282759	0.00002	9.3	724	857	-0.93
	14	0.082483	0.002566	0.282759	0.00003	9.2	729	862	-0.92

Table 5 continued

DBC-1		$^{176}\text{Yb}/^{177}\text{Hf}$	$^{176}\text{Lu}/^{177}\text{Hf}$	$^{176}\text{Hf}/^{177}\text{Hf}$	$\delta$	$\epsilon_{\text{Hf}}(\text{t})$	$T_{\text{DM1}} (\text{Ma})$	$T_{\text{DM2}} (\text{Ma})$	$f_{\text{Lu/Hf}}$
Spot									
15	0.068746	0.002232	0.282708	0.00002	7.5	797	971	—	-0.93
16	0.081757	0.002551	0.282718	0.00002	7.8	789	954	—	-0.92
17	0.052857	0.001719	0.282729	0.00002	8.4	757	914	—	-0.95
18	0.074756	0.002336	0.282770	0.00003	9.7	709	833	—	-0.93
19	0.096941	0.003034	0.282804	0.00002	10.7	671	770	—	-0.91
DBC-3									
1	0.165736	0.005188	0.282742	0.00003	7.9	815	1151	—	-0.87
2	0.092514	0.002982	0.282810	0.00002	11.0	662	869	—	-0.91
3	0.140019	0.004232	0.282739	0.00002	8.1	796	1131	—	-0.87
4	0.132669	0.004476	0.282639	0.00002	4.5	949	1450	—	-0.87
5	0.113575	0.003620	0.282751	0.00002	8.7	764	1076	—	-0.89
6	0.111253	0.003583	0.282726	0.00002	7.8	802	1156	—	-0.89
7	0.163944	0.005213	0.282819	0.00003	10.6	692	905	—	-0.89
8	0.173019	0.005334	0.282807	0.00002	10.1	713	945	—	-0.84
9	0.136595	0.004127	0.282706	0.00003	6.9	844	1234	—	-0.88
10	0.109843	0.003342	0.282844	0.00002	12.1	618	771	—	-0.90
11	0.068668	0.002288	0.282770	0.00003	9.8	708	977	—	-0.93
12	0.137637	0.004298	0.282747	0.00003	8.3	785	1109	—	-0.87
13	0.107526	0.003477	0.282766	0.00003	9.3	738	1023	—	-0.90
14	0.113243	0.003652	0.282765	0.00003	9.2	743	1031	—	-0.89
15	0.123100	0.003812	0.282804	0.00003	10.5	687	912	—	-0.89
16	0.094279	0.003013	0.282765	0.00003	9.4	729	1012	—	-0.91
17	0.116695	0.003378	0.282690	0.00003	6.6	851	1264	—	-0.90
18	0.094490	0.003009	0.282734	0.00003	8.3	776	1112	—	-0.91
19	0.111247	0.003419	0.282710	0.00003	7.3	822	1202	—	-0.90
20	0.103870	0.003372	0.282748	0.00002	8.7	763	571	—	-0.90

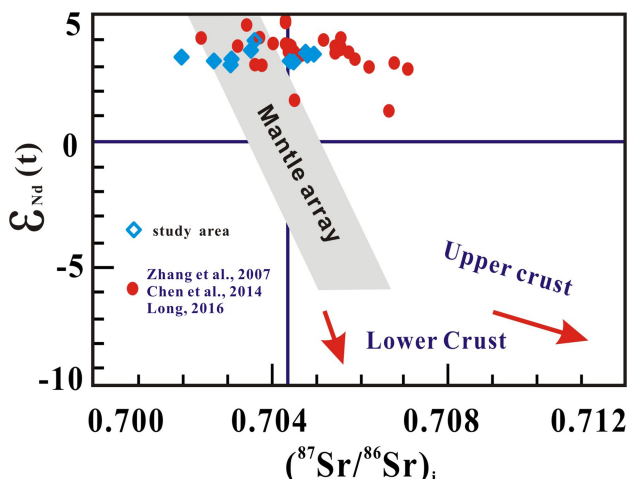


**Fig. 7** The  $(^{87}\text{Sr}/^{86}\text{Sr})_i$  vs.  $\varepsilon_{\text{Nd}}(\text{t})$  plot of the dolerites studied

under high pressure. Garnet becomes the main residual mineral phase, resulting in loss of Y and HREE in the melt, enrichment of strong incompatible elements and enrichment of MgO (Griffiths and Campbell 1990; Hill et al. 1992; Hull 1993; White and Kenzie 1995; Wang et al. 1997; Wedepohl and Baumann 1999; Wang 1998, 2001; Zhang 2001; Zhang et al. 2002).

## 6 Conclusions

Integrated U-Pb geochronology, whole-rock elemental geochemistry and Sr-Nd-Hf isotopic studies of suites of mafic dykes from the Ziyang within Shaanxi Province allow us to conclude as follows.

1. The mafic/dolerite dykes from the study area were intruded during the Early Paleozoic (Ordovician) as evidenced in the newly determined zircon U-Pb geochronological ages, of  $475.8 \pm 3.5$  Ma to  $480.7 \pm 3.9$  Ma.
2. All mafic rocks studied have an affinity to alkaline igneous suites. These are enriched in LREE [ $(\text{La/Yb})_N = 7.75\text{--}11.5$ ], and select LILE (e.g., Rb, Ba, Sr, Nb, Ta, Zr, and Hf), and Eu, and depleted in Th, U, Pb, and Ti relative to a primitive mantle. The dykes studied have low initial  $^{87}\text{Sr}/^{86}\text{Sr}$  ratios ( $0.7020\text{--}0.7050$ ), positive  $\varepsilon_{\text{Nd}}(\text{t})$  ( $3.0\text{--}4.0$ ), and  $\varepsilon_{\text{Hf}}(\text{t})$  ( $4.5\text{--}12.1$ ) values. This indicates that the dolerites studied were derived from partial melting of depleted lithospheric mantle.
3. Fractionation of olivine and clinopyroxene occurred during magma ascent, with smaller crustal contamina-

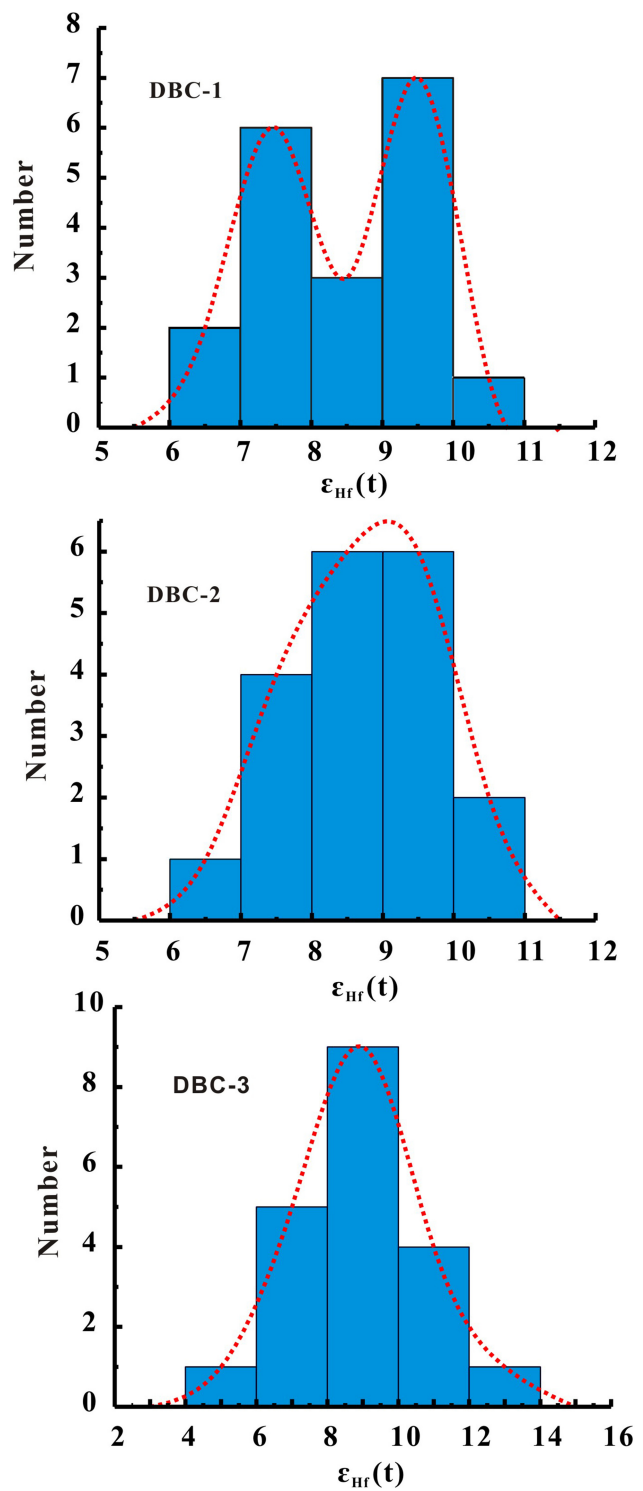


**Fig. 8** The  $\varepsilon_{\text{Hf}}(\text{t})$  histogram of the dolerites studied

tion. The geodynamic mechanism of the genetic process is mainly controlled by the mantle plume activity in Qinling.

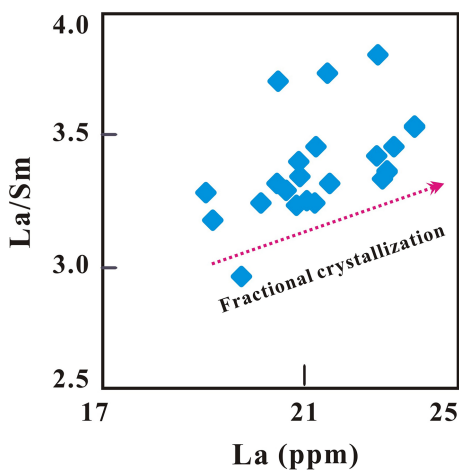


**Fig. 9** Correlation diagram of La and La/Sm for the dolerites studied

**Acknowledgements** The authors thank Dr. Shuqin Yang for assistance during the XRF analyses, Prof. Liang Qi and Xiaobiao Li for assistance during ICP-MS analyses, the technician for assistance during TIMS Sr-Nd isotopic analyses, and Profs. Xiaoming Liu for assistance during LA-ICP-MS U-Pb dating. This study was supported by the National Natural Science Foundation of China (Grant: 41573022).

## References

- Andersen T (2002) Correction of common lead in U-Pb analyses that do not report  $^{204}\text{Pb}$ . *Chem Geol* 192:59–79
- Breithopf JH (1989) Geochemical evidence for magma sources heterogeneity and activity of a mantle plume during advanced rifting in the southern Damara Orogen Namibia. *Lithos* 23:115–122
- Chen YC, Wang PA, Qin KL, Mao JW (1994) Division of metallogenetic series and regional metallogenetic law of main metal deposits in Qinling. *Miner Deposits* 13:289–298 (in Chinese with English abstract)
- Chen H, Tian M, Wu GL, Hu JM (2014) The Early Paleozoic alkaline and mafic magmatic events in southern Qinling belt, central China: evidence for the breakup of the Paleo tethyan Ocean. *Geol Rev* 60:1437–1452 (in Chinese with English abstract)
- Chen JL, He SP, Wang HL, Xu XY, Zeng ZX, Wang ZQ, Yang QR (2006) Zircon LA-ICPMS U-Pb age of mafic dykes in the area between the Qinling and the Qilian orogenic belt and its geological implications. *Acta Petrol ET Mineral* 25:455–462 (in Chinese with English abstract)
- Chu NC, Taylor RN, Chavagnac V, Nesbitt RW, Boella RM, Milton JA, German CR, Bayon G, Burton K (2002) Hf isotope ratio analysis using multi-collector inductively coupled plasma mass spectrometry; an evaluation of isobaric interference corrections. *J Anal At Spectrom* 17:1567–1574
- Condie KC (1976) Trace element geochemistry of Archean greenstone belts. *Earth Sci Rev* 12:393–417
- Davies GF, Rihards MA (1992) Mantle convection. *J Geol* 100:151–206
- Deng SB, Wang WH, Wang XJ (2003) The geological characteristics of the alkali-intermediate rocks and their ore-bearing (columbo-tantalite) feature in the Ziyang-Langao areas. *Geol Shaanxi* 21:19–32 (in Chinese with English abstract)
- Ewing RC (1994) The metamict state: 1993—the centennial. *Nucl Instrum Methods Phys Res Sect B* 91:22–29
- Feng GY (2012) *Geochronology, Geochemistry and Geodynamic Significance of Late Paleozoic-Mesozoic Basic Rocks in Liaoji Area*. PhD thesis of the Institute of Geochemistry, Chinese Academy of Science
- Hofmann E (1988) Chemical differentiation of the earth: the relationship between mantle, continental crust, and oceanic crust. *Earth Planet Sci Lett* 90:297–314
- Gree TH (1995) Significance of Nb/Ta as an indicator of geochemical processes in the crust-mantle system. *Chem Geol* 120:347–359
- Griffiths RW, Campbell IH (1990) Stirring and structure in mantle starting plumes. *Earth Planet Sci Lett* 99:66–78
- Guo F, Fan WM, Wang YJ, Zhang M (2004) Origin of early Cretaceous calc-alkaline lamprophyres from the Sulu orogeny eastern China: implications for enrichment processes beneath continental collisional belt. *Lithos* 78:291–305
- Hall HC (1982) The importance and potential of mafic dyke swarms in studies of geodynamic process. *Geosci Canada* 9:145–154
- Hill RI, Campbell IH, Davies GF (1992) Mantle plumes and continental tectonics. *Science* 256:186–193
- Hofmann AW, White WM (1982) Mantle plumes from ancient oceanic crust. *Earth Planet Sci Lett* 57:421–436
- Hull RI (1993) Mantle plumes and continental tectonics. *Lithos* 30:193–206
- Iizuka T, Hirata T (2005) Improvements of precision and accuracy in in-situ Hf isotope microanalysis of zircon using the laser ablation-MC-ICPMS technique. *Chem Geol* 220:121–137
- Kuang YQ, Zhang BR, Ouyang JP (1995) The regional crustal mobility reflected by the geochemistry of Paleozoic sedimentary rocks in south Qinling. *Acta Petrol Sin* 11:203–212 (in Chinese with English abstract)
- Li XH (1990) Preliminary study on the genesis of basic dikes in Zhuguangshan rock mass—evidence from Sr, Nd and O isotopes. *Chin Sci Bull* 35:1247–1249 (in Chinese)
- Li FJ (2009) The rock geochemistry characteristics and tectonic implications of mafic dyke swarms and syenite porphyry veins in Zhenba eastern area, southern Shaanxi province, the master's degree thesis of Chang'an University 1–81 (in Chinese with English abstract)
- Li FJ, Yang J (2011) Tectonic meaning of mafic dyke swarms in Zhenba eastern area in Shannan. *J Sichuan Univ Sci Eng* 24:238–243 (in Chinese with English abstract)
- Li JH, He WJ, Qian XL (1997) Genetic mechanism and tectonic setting of Proterozoic mafic dyke swarm: its implication for paleo-plate reconstruction. *Geol J China Univ* 3:272–280 (in Chinese with English abstract)
- Li ZX, Li XH, Kinny PD (1999) The breakup of Rodinia: did it start with a mantle plume beneath south China? *Earth Planet Lett* 173:171–181
- Liu ZQ (2008) The regional tectonic characteristic and their evolution of Zhenba-Ziyang, southern Shaanxi. The master's degree thesis of Chang'an University, 1–89 (in Chinese with English abstract)
- Liu S, Hu RZ, Zhao JH, Feng CX (2004) K-Ar ages of Mesozoic mafic dyke rocks and crustal extension in Shandong Province, eastern China. *Acta Geol Sin* 78:1207–1213
- Liu S, Zou HB, Hu RZ, Zhao JH, Feng CX (2006) Mesozoic mafic dikes from the Shandong Peninsula, NCC: petrogenesis and tectonic implications. *Geochem J* 40:181–195
- Liu XM, Gao S, Diwu CR, Yuang HL, Hu ZC (2007) Simultaneous *in-situ* determination of U-Pb age and trace elements in zircon by LA-ICP-MS in  $20\mu$  spot size. *Chin Sci Bull* 52:1257–1264
- Liu S, Hu RZ, Gao S, Feng CX, Qi L, Zhong H, Xiao TF, Qi YQ, Wang T, Coulson IM (2008a) Zircon U-Pb geochronology and

- major, trace elemental and Sr-Nd-Pb isotopic geochemistry of mafic dykes in western Shandong Province, east China: Constrains on their petrogenesis and geodynamic significance. *Chem Geol* 255:329–345
- Liu S, Hu RZ, Gao S, Feng CX, Qi YQ, Wang T, Feng GY, Coulson IM (2008b) U-Pb zircon age, geochemical and Sr-Nd-Pb-Hf isotopic constraints on age and origin of alkaline intrusions and associated mafic dikes from Sulu orogenic belt, Eastern China. *Lithos* 106:365–379
- Liu S, Hu RZ, Gao S, Feng CX, Yu BB, Feng GY, Qi YQ, Wang T, Coulson IM (2009) Petrogenesis of late Meozoic mafic dykes in the Jiaodong peninsula, eastern NCC and implications for the foundering of lower crust. *Lithos* 113:621–639
- Liu S, Su WC, Hu RZ, Feng CX, Gao S, Coulson IM, Wang T, Feng GY, Tao Y, Xia Y (2010a) Geochronological and geochemical constraints on the petrogenesis of alkaline ultramafic dykes from southwest Guizhou Province, SW China. *Lithos* 114:253–264
- Liu S, Hu RZ, Gao S, Feng CX, Feng GY, Coulson IM, Li C, Wang T, Qi YQ (2010b) Zircon U-Pb age and Sr-Nd-Hf isotope geochemistry of Permian granodiorite and associated gabbro in the Songliao Block, NE China and implications for growth of juvenile crust. *Lithos* 114:423–436
- Liu S, Hu RZ, Yang YH, Feng CX, Qi YQ, Wang T (2010c) Distribution and significance of the mafic dyke swarms since Mesozoic in the NCC. *Geol Bull China* 29:259–267
- Liu S, Hu RZ, Gao S, Feng CX, Coulson IM, Feng GY, Qi YQ, Yang YH, Yang CG, Tang L (2012a) U-Pb zircon age, geochemical and Sr-Nd isotopic data as constraints on the petrogenesis and emplacement time of the Precambrian mafic dyke swarms in the NCC. *Lithos* 140–141:38–52
- Liu S, Hu RZ, Gao S, Feng GY, Qi YQ, Coulson IM, Yang YH, Yang CG, Tang L (2012b) Geochemical and isotopic constraints on the age and origin of mafic dikes from Eastern Shandong province, Eastern NCC, China. *Int Geol Rev* 54:1389–1400
- Liu S, Feng CX, Jahn BM, Hu RZ, Gao S, Feng GY, Lai SC, Yang YH, Qi YQ, Coulson IM (2013a) Geochemical, Sr-Nd isotopic, and zircon U-Pb geochronological constraints on the petrogenesis of Late Paleoproterozoic mafic dykes within the northern NCC, Shanxi Province, China. *Precambr Res* 206:182–192
- Liu S, Feng CX, Jahn BM, Hu RZ, Gao S, Coulson IM, Feng GY, Lai SC, Yang YH (2013b) Zircon U-Pb age, geochemical, and Sr-Nd-Hf isotopic constraints on the origin of mafic dykes in the Shaanxi Province, NCC, China. *Lithos* 175–176:244–254
- Liu S, Feng CX, Jahn BM, Hu RZ, Gao S, Coulson IM, Feng GY, Lai SC, Yang YH, Tang L (2013c) Geochemical, Sr-Nd-Pb isotope, and zircon U-Pb geochronological constraints on the origin of Early Permian mafic dykes, northern NCC. *Int Geol Rev* 55:1626–1640
- Liu S, Hu RZ, Feng CX, Gao S, Feng GY, Lai SC, Qi YQ, Coulson IM, Yang YH, Yang CG, Tang L (2013d) U-Pb zircon age, Geochemical, and Sr-Nd-Pb isotopic constraints on the age and origin of mafic dykes from eastern Shandong Province, eastern China. *Acta Geol Sin* 87:1045–1057
- Liu S, Hu RZ, Gao S, Feng CX, Coulson IM, Feng GY, Qi YQ, Yang YH, Yang CG, Tang L (2013e) Zircon U-Pb age and Sr-Nd-Hf isotopic constraints on the age and origin of Triassic mafic dykes, Dalian area, Northeast China. *Int Geol Rev* 55:249–262
- Liu S, Feng CX, Jahn BM, Hu RZ, Gao S, Coulson IM, Feng GY, Lai SC, Yang CG, Yang YH (2013f) Zircon U-Pb age, geochemical, and Sr-Nd-Hf isotopic constraints on the origin of mafic dykes in the Shaanxi province, NCC, China. *Lithos* 175–176:244–254
- Liu S, Feng CX, Hu RZ, Zhai MG, Gao S, Lai SC, Yan J, Coulson IM, Zou HB (2015) Zircon U-Pb geochronological, geochemical, and Sr-Nd isotope data for early Cretaceous mafic dykes in the Tancheng-Lujiang Fault area of the Shandong province, China: Constraints on the timing of magmatism and magma genesis. *J Asian Earth Sci* 98:247–260
- Liu S, Feng CX, Zhai MG, Hu RZ, Lai SC, Chen JJ, Yan J (2016) Zircon U-Pb age, geochemical, and Sr-Nd-Hf isotopic constraints on the origin of early Cretaceous mafic dykes from western Shandong province, eastern NCC. *Acta Petrol Sin* 32:629–645
- Liu S, Feng CX, Feng GY, Xu MJ, Coulson IM, Guo XL, Guo Z, Peng H, Feng Q (2017a) Timing, mantle source and origin of mafic dykes within the gravity anomaly belt of the Taihang-Da Hinggan gravity lineament, central NCC. *J Geodyn* 109:41–58
- Liu S, Feng CX, Feng GY, Xu MJ, Guo XL, Feng Q, Yan J, Guo Z (2017b) Zircon U-Pb age, geochemical and Sr-Nd-Pb isotopic data: constraints on the genetic model of the mafic dykes from the NCC. *Acta Petrol Sin* 33:1667–1685
- Liu S, Feng CX, Santosh M, Feng GY, Coulson IM, Xu MJ, Guo Z, Guo XL, Peng H, Feng Q (2018) Integrated elemental Sr-Nd-Pb-Hf isotopic studies of Mesozoic mafic dykes from the eastern NCC: implications for the dramatic transformation of lithospheric mantle. *J Geodyn* 114:19–40
- Long JS (2016) The geochemical characteristics and geological significance of the basin dyke swarms and syenite porphyry veins in the Ziyang, south Shaanxi. The master's degree thesis of Chang'an University
- Ludwig KR (2003) ISOPLOT 3.0: a geochronological Toolkit for Microsoft Excel, Berkeley Geochronology Center. Special Publication No. 4
- Machado N, Simonetti A (2001) U-Pb dating and Hf isotopic composition of zircon by laser-ablation MC-ICP-MS. In: Ylvester P (ed) Laser ablation-ICPMS in the Earth. Science: principles and applications. Mineralogical Association of Canada, St John's Newfoundland, pp 21–146
- Meng Q, Zhang C (1999) Timing of collision of the North and South China blocks: controversy and reconciliation. *Geology* 27:123–136
- Morgan WJ (1971) Convection plumes in the lower mantle. *Nature* 230:42–43
- Peng P, Zhai MG, Zhang HF, Zhao TP, Ni ZY (2004) Geochemistry and geological significance of the 18Ga mafic dyke swarms in the NCC: an example from the Juncture of Shanxi, Hebei and Inner Mongolia. *Acta Petrol Sin* 20:439–456 (in Chinese with English abstract)
- Qi L, Hu J, Gregoire DC (2000) Determination of trace elements in granites by inductively coupled plasma mass spectrometry. *Talanta* 51:507–513
- Qi SJ, Li HM, Li Y, Hu SG (1999) Some important ore deposit series in Qinling range. *J Xi'an Eng Univ* 21:28–35 (in Chinese with English abstract)
- Shao JA, Zhang LQ (2002) Mesozoic dyke swarms in the north of North China. *Acta Petrol Sin* 18:312–318 (in Chinese with English abstract)
- Sun SS, McDonough WF (1989) Chemical and isotopic systematics of oceanic basalts: implications for mantle composition and processes. In: Saunders AD, Norry MJ (eds) Magmatism in Oceanic Basins Sprc Publ Geol Soc Lond 42:313–345
- Tang L (2013) Geochronology and Geochemistry of Mesozoic Basic Dykes and Acidic Rocks in Hebei and Inner Mongolia. Mater thesis of the Institute of Geochemistry, Chinese Academy of Science
- Tang YZ, Qi W, Liu SW, Hou MT (2007) Paleozoic hydrothermal sedimentary basin and hydrothermal sedimentary mineralization in the southern Qinling. *Geol China* 34:1991 (in Chinese with English abstract)
- Thompson RN, Gibson Sally A (2019) Subcontinental mantle plumes, hotspots and pre-existing thinspots. *J Geol Soc Lond* 148:973–977

- Trevor HG (1995) Significance of Nb/Ta as an indicator of geochemical processes in the crust-mantle system. *Geology* 12:347–359
- Tu HK (2006) Gold-copper deposits geology and mineralization condition of Ankang region. *Geol Chem Miner* 28:87–93 (in Chinese with English abstract)
- Wang DH (1998) Mantle plume and its mineralization. Earthquake Publishing House (in Chinese with English abstract)
- Wang DH (2001) Basic concept, classification, evolution of mantle plume and large scale mineralization-probe into southwestern China. *Earth Sci Front* 8:67–72 (in Chinese with English abstract)
- Wang YB (2007) Geological characteristics and significance of Early Paleozoic alkali volcanic in south Qinling, Langao-Pingli, Shaanxi province. The master's degree thesis of Chang'an University, 1–76 (in Chinese with English abstract)
- Wang RM, Chen ZZ, Lai XY (1997) Archean geotectonic transition of systems from mantle plume to plate tectonics in North China. *J China Univ Geosci* 22:317–321 (in Chinese with English abstract)
- Wang TH, Mao JW, Wang YB (2008) Research on SHRIMP U-Pb chronology in Xiaoqinling-Xionger'shan area: the evidence of delamination of lithosphere in Qinling orogenic belt. *Acta Petrol Sin* 24:1273–1287 (in Chinese with English abstract)
- Wang CZ, Yang KG, Xu Y, Cheng WQ (2009) Geochemistry and LA-ICP-MS zircon U-Pb age of basic swarms in north Dabamoutatins and its tectonic significance. *Geol Sci Technol Inf* 28:19–26 (in Chinese with English abstract)
- Wedepohl KH, Bamann A (1999) Central European Cenozoic plume volcanism with OIB characteristics and indications of a lower mantle source. *Contrib Miner Petrol* 136:225–239
- Wei D, Chen XM, Peng XJ (2016) Geological characteristics and metallogenetic conditions of Barite ore belt at south margin of Pinli dome in northern Dabashan. *Northwest Geol* 49:214–223 (in Chinese with English abstract)
- White RS, Renzie DM (1995) Mantle plumes and flood basalts. *J Geophys Res* 100(B9):17543–17585
- Woodhead J, Hergt J, Shelley M, Eggins S, Kemp R (2004) Zircon Hf-isotope analysis with an excimer laser, depth profiling, ablation of complex geometries, and concomitant age estimation. *Chem Geol* 209:21–135
- Wu FY, Walker RJ, Yang YH, Yuan HL, Yang JH (2006) The chemical-temporal evolution of lithospheric mantle underlying the NCC. *Geochim Cosmochim Acta* 7:51–503
- Xie GQ (2003) Late Mesozoic and Cenozoic Mafic Dikes (bodies) from Southeastern China: geological and geochemical characteristics and its geodynamics-a case of Jiangxi Province. PhD thesis of Institute of Geochemistry, Chinese Academy of Science
- Xie QQ, Zhao YL, Zhang HX, Chen TH, Xu XC, Xue HM, Zhao JX (2014) Zircon U-Pb dating and trace elements geochemistry of the Gaotan gabbro from Ziyang county, Shaanxi province. *Chin J Geol* 49:456–471
- Xu XY, Xia LQ, Xia ZC (2001) Geochemical characteristics and petrogenesis of the Early Paleozoic alkali lamprophyre complex from Langao county. *Acta Geosci Sin* 22:55–60 (in Chinese with English abstract)
- Wu SH, Liu JJ, Zhai DG (2010) Geochemical characteristics of metallogenetic fluids in huangbaishawan barium deposit, Ziyang, Shaanxi. *Miner Deposit* 29:615–616 (in Chinese)
- Yang SN (1985) The evolution of Qinling intercontinental rift system in Paleozoic. *Earth Sci* 10:53–62 (in Chinese with English abstract)
- Yan YX (2005) Petrogeochemistry and Sr, Nd and Pb isotope geochemistry of alkali-basic dike swarms in Ziyang-Langao area, Shaanxi Province. The master's degree thesis of Northwest University 1–57 (in Chinese)
- Yang CG (2012) Geochronological and geochemical characteristics of basic diamonds in the southern margin of north China plate. Mater thesis of the Institute of Geochemistry, Chinese Academy of Science
- Yang YH (2013) Geochronology and geochemistry of mesozoic basic dyke group in NCC. PhD thesis of the Institute of Geochemistry, Chinese Academy of Science
- Yuan HL, Gao S, Liu XM, Li HM, Gunther D, Wu FY (2004) Accurate U-Pb age and trace element determinations of zircon by laser ablation-inductively coupled plasma mass spectrometry. *Geostand Geoanal Res* 28:353–370
- Zeng R, Liu SW, Xue CJ, Gong JX (2007) Mineralization in evolution of Paleozoic basins in south Qinling. *J Earth Sci Environ* 29:234–239 (in Chinese with English abstract)
- Zhang BR (2001) Magmatic activites from plume-source in the Qinlinorogenic belt and its dynamic significance. *Earth Sci Front* 8:55–66 (in Chinese with English abstract)
- Zhang JJ, Zheng YD (1999) Stages and dating of the development of the Xiaoqinling metamorphic core complex. *Acta Geol Sin* 73:190 (in Chinese)
- Zhang GW, Zhang BR, Yuan XC and Xiao QH (2001) Continental dynamics of Qinling orogenic belt. Science Press (in Chinese with English abstract)
- Zhang CL, Gao S, Yuan HL, Zhang GW, Yan YX, Luo JL, Luo JH (2007) Early Paleozoic mantle properties in South Qinling: Sr-Nd-Pb isotopic evidence from ultramafic, mafic dikes and volcanic rocks. *Sci China (D)* 37:857–865 (in Chinese)
- Zhang GS, Liu SW, Han WH, Zheng HY (2017) Baddeleyite U-Pb age and geochemical data of the mafic dykes from south Qinling: constraints on the lithospheric extension. *Geochem J* 52:272–285
- Zhan JL, Chen GC, Li ZH, Wang JC, Zhang QS, Kong WN, Zhang SA (2012) Filling sequence and structural evolution in the early Paleozoic basin of southern Qinling Mountains. *Geol Shaanxi* 30:38–45 (in Chinese with English abstract)
- Zhang X (2010) The dynamic mechanism and geological significance of mafic intrusion in the Ziyang-Zhenba area, south Qinling. The master's degree thesis of Chang'an University, 1–79 (in Chinese with English abstract)
- Zhang CY, Chen QS, Yang CH (2012) Diabase mass and metallogenetic condition of titanomagnetite in ankang area of Shaanxi province. *Gansu Geol* 21:39–45 (in Chinese with English abstract)
- Zhao JH (2004) Chronology and geochemistry of mafic rocks from Fujian Province: implications for the mantle evolution of SE China since Late Mesozoic. PhD thesis of Institute of Geochemistry, Chinese Academy of Science
- Zhao JH, Hu RZ, Liu S (2004) Geochemistry, petrogenesis, and tectonic significance of Mesozoic mafic dikes, Fujian Province, Southeastern China. *Int Geol Rev* 6:528–541
- Zhu WD (2017) Geological characteristics and genesis of Dangshan gold deposit in Shaanxi province, China. The master's degree thesis of East China University of Technology 1–54 (in Chinese with English abstract)
- Zou XW, Duan QF, Tang CY, Cao L, Cui S, Zhao WQ, Xia J, Wang F (2011) SHRIMP zircon U-Pb dating and lithogeochemical characteristics of diabase from Zhenping area in north Daba Mountain. *Geol China* 38:282–291 (in Chinese with English abstract)